Measurement of fission fragments and neutron beam spots using a fission TPC on a white light neutron source*

Jia-Jun Zhang,[1,2] Jun Xiao,[2] Jing-Jing Xiao,[3] Jun-Jie Sun,[2] Tai-Ping Peng,[2] and Pu Zheng[2,†]

[1]*Bio-Med Informatics Research Center, Clinical Medical Research Center, Second Affiliated Hospital, Army Medical University, Chongqing 400037, China*

[2]*Institute of Nuclear Physics and Chemistry, China Academy of Engineering Physics, Mianyang 621000, China*

[3]*Bio-Med Informatics Research Centre, Clinical Medical Research Center, Second Affiliated Hospital, Army Medical University, Chongqing 400037, China*

Neutrons emitted from white light neutron sources have a wide energy range and produce a wide variety of particle types after interacting with the target. The ability to accurately distinguish different particles and identify fission fragments is of crucial importance for measuring the fission cross-section. Compared with other detectors, Time Projection Chamber (TPC) has a larger sensitive volume and can reconstruct the three-dimensional track of incident particles by detecting electrons generated by ionizing the working gas. TPC can also record the energy deposition process of particles, thereby measuring their ionization ability dE/dx. Based on these two characteristics, TPC possesses strong particle identification capabilities, thus it has extensive application prospects in the measurement of the fission cross-section. This paper introduces a fission TPC for measuring neutron-induced fission cross-sections. The preliminary experimental results indicate that fission fragments can be effectively distinguished and the size of the neutron beam spot can be accurately measured.

Keywords: Time Projection Chamber; Fission cross-section; Particle track reconstruction; Particle identification; Neutron beam spot.

I. INTRODUCTION

With the widespread application of nuclear fission in new energy, national defense, astrophysics and other fields, people have put forward higher requirements for the accuracy of fission cross-section data. The higher accuracy requirements have also driven the development of detectors. Traditional measurement methods, such as fission chambers, are limited by their own structure and measurement principles, and the accuracy of measuring the fission cross-sections of major actinide nuclides is always between 3% and 5% [1]. Previous methods have found it difficult to achieve higher levels of measurement accuracy. At present, the evaluation of fission cross-sections based on a large number of experimental datasets can achieve a very accurate level, and in some cases can even reach an uncertainty of 1% [1]. But in the fast neutron region (where the incident neutron energy ranges from 100 keV to 14 MeV), the measurement accuracy of the fission cross section for major fission nuclides such as ^{235}U and ^{238}U is usually between 3% and 5%. In applications such as reactors, national defense, and nuclide synthesis calculations, higher requirements have been put forward by people for the measurement accuracy of fission cross-sections. Through extensive research on the impact of uncertainty, it has been concluded that a precision of 1% or higher is required [2]. In addition, as mentioned earlier, the uncertainty of the system also constrains the measurement accuracy. Consequently, with the aim of further enhancing the measurement accuracy of fission cross-sections, new measurement methods and detectors are urgently needed.

The Time Projection Chamber (TPC) was first proposed and invented by Nygren et al. in 1974, and was soon applied to the PEP-4 experimental detection in the SLAC Electron Positron Collider [3]. TPC is essentially a kind of gas drift detector. It consists of drift area of different shapes and readout detectors with position (X-Y plane) and time measurement functions. The electron drift time is capable of providing the information in the Z direction. A certain magnetic field can be applied parallel to the electric field direction to measure the momentum of the incident particles. Magnetic fields can also suppress transverse diffusion during electron drift, improving the spatial resolution of tracks. In contrast to other detectors, TPC detectors possess a sensitive volume that is large enough to detect and reconstruct the three-dimensional track of incident charged particles. It can record the energy deposition process of particles, thus measuring the ionization capacity dE/dx of particles.

Based on these two characteristics, TPC has excellent performance in identifying particle types. As a result, in numerous large-scale high-energy particle experiments, TPC is used as the central track detector. Notable among them are ALEPH [4], DELPHI [5] in LEP experiments, STAR [6] in BNL, and ALICE [7] in LHC. The CERN (European Organization for Nuclear Research) extensively deploys TPC detectors in experiments related to the LHC (Large Hadron Collider). In the ALICE experiment, TPC is responsible for detecting the massive charged particles generated in heavy ion collisions. Researchers have combined advanced MPGDs (Micro-Pattern Gas Detectors) technology with TPC to achieve extremely high spatial resolution, reaching sub millimeter levels.

For the ILC (International Linear Collider), researchers propose a TPC based on GEM (Gas Electron Multiplier), readout system as the main tracking detector for the DESY II synchrotron [8,9]. The TPC was designed in accordance with the experimental requirements related to ILC for a detailed

* Supported by the Youth Doctoral Talent Incubation Program of the Second Affiliated Hospital of Army Medical University (No. 2024YQB060)

† Corresponding author, Pu Zheng, Mianyang China, 15823535190, 646764732@qq.com.

study of the properties of the Higgs boson, which demands more accurate measurements of the momentum of charged particles. This TPC can achieve a momentum resolution of $\Delta(1/P_T) = 10^{-4}GeV^{-1}$. With 200 position measurements performed along the particle track, this TPC provides excellent pattern recognition capability and nearly 100% low momentum tracking efficiency.

TPC detection technology is also applicable for measuring the polarization of γ rays with outstanding angular accuracy and sensitivity within the MeV-GeV energy range through the conversion of photons into e^+e^- pairs. Therefore, Shaobo Wang et al. [10] built a prototype of the HARPO (Hermetic Argon Polarimeter) and tested it in a polarized photon beam at the NewSUBARU facility in Japan. The experiment measured low-energy polarization asymmetries of cosmic γ rays. The range of angular momentum measured using TPC is one order of magnitude higher than that of Fermi-LAT (Fermi Large Area Telescope).

The CEE-TPC planned by the CEE (CSR External-target Experiment) cooperation group has entered the prototype production stage, with the goal of achieving full space measurement of charged ion products generated in heavy ion collisions [11,12]. The TPC will be installed in the low-temperature high-density nuclear material measurement spectrometer on the Lanzhou heavy ion accelerator device, combined with a multiwire proportional chamber to form the main track detector of the spectrometer, for measuring the three-dimensional tracks of charged particles.

The search for NLDBD (Neutrinoless Double Beta Decay) is considered a reliable way to probe the nature of neutrinos. The PandaX-III experiment, located in the CJPL (China JinPing Underground Laboratory), is the first large-scale project to use TPC to search for NLDBD of ^{136}Xe [13,14]. This TPC is filled with 200 kg of high-pressure mixed gas (^{136}Xe and trimethylamine) and uses MICROMEGAS (MICRO Mesh Gaseous Structure) as the readout system. The TPC is able to identify two electronic events from the γ background with a high confidence level. At the Q value of β decay, the energy resolution can reach about 3% FWHM. At present, the system is actively being developed and improved.

The technology of using TPC for ultra-low background detection of α and β proposed by the team from the University of Science and Technology of China has achieved good results [15]. This TPC can achieve counting, α spectrum measurement, and pollution distribution imaging under extremely low background radiation. Under unshielded conditions, the background count rate of α is reduced by more than 10 times compared to similar commercial products.

The TPC detection technology also has a very broad application prospect in the direction of fission cross-section measurement. Traditional fission chambers only record the total energy deposited by fission events in the fission chambers. However, different types of particles, such as fission fragments, alpha particles, and protons scattered out of the target chamber, may generate events with similar energies, which leads to the inability of the fission chambers to identify these types of particles. By incorporating the entire ionization process of charged particles within its effective volume, the fission TPC can provide more effective particle identification capabilities. The fission TPC can record the deposited energy and the length of the ionization tracks, which depend on the mass and charge of each particle. Heavy fission fragments will lose energy rapidly and thus leave shorter ionization tracks, while α particles have longer tracks. When the ionization tracks are plotted as a function of distance, there is a distinct peak (Bragg peak) in the ionization track of α particles, indicating the max energy loss. By employing the ionization information of each particle, with Bragg peak data included, the fission TPC can effectively identify particle types.

The NIFFTE (Neutron Induced Fission Fragment Tracking Experiment) collaboration is at the forefront of applying TPC to fission cross-section measurement [16,17]. This fission TPC uses MICROMEGAS (MICRO Mesh Gaseous Structure) as the readout detector and has 5952 readout pads. It does not require a magnetic field to control diffusion because the drift distance is short (about 54 mm). The working gas is an argon-isobutane mixture at a pressure of 550 Torr. Recently, they have measured the ^{239}Pu(n, f)/^{235}U(n, f) cross-section ratio (0.2 MeV to 100 MeV) using this TPC, and the uncertainty of the results can reach about 1%. They also used NIFFTE TPC to measure the α/SF branching ratio of $252Cf$ and obtained experimental results that were very close to the reference value [18].

The CSNS (Chinese Spallation Neutron Source) team has also done good work in fission TPC. One of the main purposes of the MTPC (Multi-purpose TPC) developed by the CSNS is also to accurately measure the fission cross-section [19-21]. MTPC also uses MICROMEGAS as the readout detector, with a total of 1519 readout pads. The MTPC team has currently measured the cross-section of ^{232}Th(n, f) at multiple energy points (4.50 MeV to 5.40 MeV), and the results are consistent with the evaluation data [22,23]. The relevant research team has also developed an open-source program framework called BLUET for simulation and data analysis based on MTPC, providing a convenient and efficient sharing platform for TPC data analysis work of different research teams.

The INPC-TPC, independently developed by the Institute of Nuclear Physics and Chemistry of the Chinese Academy of Engineering Physics, is the third TPC detection system in the world specifically designed for neutron-induced cross-section measurement, following NIFFTE TPC and MTPC. Its main purpose is to perform high-precision fission cross-section measurements (100 keV to 14 MeV) on actinide nuclides such as ^{235}U and ^{239}Pu, with the expectation of reducing measurement uncertainty to 1% or less. To achieve such high measurement accuracy, the selection of reference cross-section is crucial. As we know, most neutron induced reaction cross-sections are measured relative to the standard cross-section, and few reaction cross-sections can be directly measured. Therefore, the measurement accuracy of fission cross-section also depends to some extent on the accuracy of the standard cross-section. At present, the fission cross-section measurement of commonly used actinide elements is usually based on the ^{235}U(n, f) cross-section as the reference cross-section for relative measurement, so the uncertainty of

the measurement results is difficult to reduce to a lower level. We design the H (n, n) cross-section as the reference cross-section because the uncertainty of the H (n, n) cross-section is currently the lowest among all standard cross-sections (about 0.2%) [24]. It makes the goal we have set theoretically feasible. We have completed the design and development of the entire system, and conducted testing experiments on the white light neutron source of CSNS. The main body of CSNS includes a 1.6GeV fast cycle proton synchrotron, an 80MeV negative hydrogen linear accelerator, as well as a central target station and different neutron beam line pipelines [25-27]. After protons bombard tungsten targets, some of the neutrons produced will rebound. CSNS separately leads out the neutrons flowing back along the target channel, creating a back-streaming white neutron beam (Back-n), which leads to two experimental terminals [28]. Back-n has the characteristics of high flight time resolution and high flux (up to $2 \times 10^7 cm^{-2}s^{-1}$), and has a wide energy range (0.5 eV to 200 MeV) and high energy resolution.

This paper introduces the measurement principle and structural design of INPC-TPC, and analyzes the experimental data collected on Back-n. From the results, it can be seen that INPC-TPC can effectively identify fission fragments and perform high-precision measurements on neutron beam spots.

II. MEASUREMENT PRINCIPLES AND SYSTEM STRUCTURE

The structure of the INPC-TPC's main chamber is presented in Figure 1. It mainly consists of a gas distribution system, field cage, GEM (Gas Electron Multiplier), readout PCB and preamplifier array. Different from the fission TPC built by NIFFTE and CSNS, INPC-TPC uses GEM as the readout detector, while NIFFTE TPC and MTPC use MICROMEGAS. Compared with MICROMEGAS, GEM has superior gain uniformity and is less susceptible to ignition [29]. The width of the electronic signal amplified by GEM avalanche is very narrow (as low as 20 ns), therefore it has better track resolution ability. Compared with the traditional TPC, the TPC based on GEM readout has a better spatial resolution. A typical GEM is composed of a 50–70 μm thick polyimide film, with copper cladding on both sides [30]. Holes with diameters ranging from 30 to 50 μm are etched between the copper layers using lithography and acid etching techniques [30]. In practical applications, a high voltage of hundreds of volts is applied between the two copper layers, creating a strong electric field within the small holes. A single electron entering these small holes will be amplified hundreds or thousands of times due to the avalanche effect.

The particles which are generated by the target continuously ionize the working gas in a uniform electric field provided by the field cage, and thus produce drift electrons. GEM performs avalanche amplification on drifting electrons. Finally, the two-dimensional readout PCB collects electrons and provides signals with amplitude and time information. The readout PCB (diameter 560 mm) consists of 4608 readout pads, as shown in Figure 1. The pad's size has a significant effect on the particle identification performance. During the early development process, we simulated the identification effects of four pad sizes, namely hexagons with diameters of 1 mm, 2 mm, 3 mm, and 4 mm respectively. The relevant simulation results show that the smaller the pad size is, the better the identification effect will be. However, when the pad size is too small, it also brings difficulties to the engineering implementation. For a detailed analysis, please read reference [31]. After comprehensive consideration, we have chosen a pad diameter of 2 mm, with a spacing of 125 μm between each pad. Every pad is connected individually to a preamplifier, and the total of 4608 channels forms a preamplifier array. We can obtain the position information of the electron cluster in the X-Y plane based on the position of the pad which generates the signal. Additionally, the position information of the electron cluster in the Z direction can be determined by multiplying the drift time by the drift velocity. The drift velocity of electrons is obtained through Garfield++ simulation. Using the position distribution and signal amplitude of drift electrons in three-dimensional space, we can reconstruct particle tracks and energy loss processes, and thereby achieve particle identification. Previously, we have already used α particles emitted from the ^{241}Am source to measure the position resolution of the system. When the voltage of the GEM was 1300 V, the position resolution in the X-Y plane was 122 μm, which was obtained by performing Gaussian fitting on the residual distribution curve within the X-Y plane.

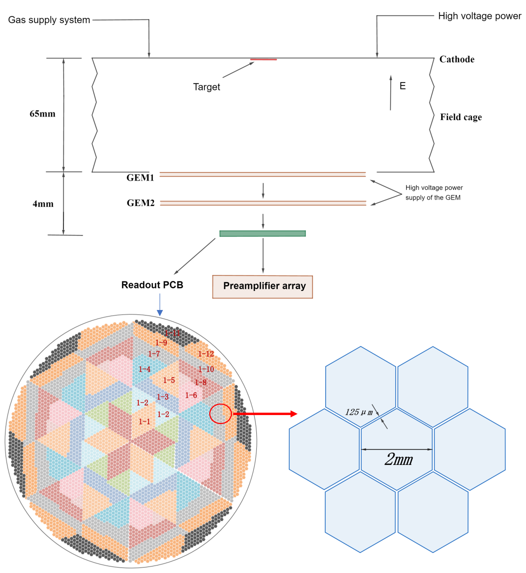

Fig. 1. The structure of the main chamber and readout PCB.

We make use of the H (n, n) elastic scattering cross-section as the reference cross-section, and the calculation formula for the fission cross-section is shown below.

$$\frac{\sigma_x}{\sigma_H} = \frac{\epsilon_H}{\epsilon_x} \cdot \frac{\Phi_H}{\Phi_x} \cdot \frac{N_H}{N_x} \cdot \frac{\sum_{XY}(B_{H,i} \cdot n_{H,i})}{\sum_{XY}(B_{x,i} \cdot n_{x,i})} \cdot \frac{\omega_x}{\omega_H} \cdot \frac{C_x}{C_H}. \quad (1)$$

where x is the nuclide to be measured, σ is the fission cross-section, ϵ is the detection efficiency, Φ is the neutron flux, and

N is the total number of target nuclei. B_i and n_i represent the number of target nuclei and neutron flux at position i in the discretized space. ω is the dead time correction coefficient, and C is the number of particles produced by the reaction. According to equation (1), the main physical parameters we need to measure include neutron flux and distribution Φ, the number and distribution of target nuclei B_i, and the number of reaction event C. The calculation of the number of target nuclei can be achieved by measuring the spontaneous decay of α particles, as detailed in reference [32]. The measurement of neutron flux can be inferred by measuring recoil protons. There is a huge difference in energy loss between fission fragments and protons. Due to the significant difference in energy loss between fission fragments and protons, using a single chamber to detect fission fragments and protons requires a high dynamic range of the system. We design a symmetrical dual-chamber structure to achieve simultaneous measurement of protons and fission fragments separately. Each chamber sets a fixed gain based on the particles that need to be measured. The dual-chamber structure and the internal configuration of the main chamber are depicted in Figure 2.

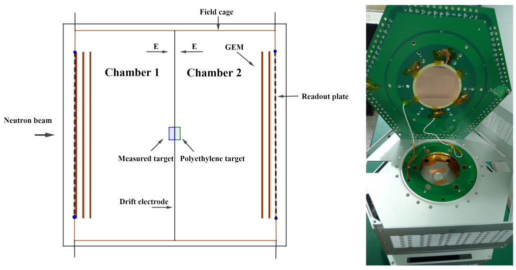

Fig. 2. The structure of the dual-chamber system (left) and the main chamber (right).

The two chambers are filled with working gas, and the target to be measured (such as ^{235}U) is placed on the cathode plate in Chamber 1. Then we place the reference target (such as polyethylene) in the position corresponding to the target to be measured in Chamber 2. The neutron beam enters Chamber 1 and hits the target, producing fission fragments and α particles. Polyethylene targets serve as radiating body for measuring neutrons. After hitting the target, neutrons will undergo elastic collisions with the hydrogen atoms, resulting in the emission of recoil protons. The neutron flux on the target can be calculated based on the count of recoil protons. Then we can calculate the fission cross-section ratio based on the elastic scattering cross-section of hydrogen, the number of fission events, and the number of target nuclei.

III. TARGET AND ELECTRONICS SYSTEMS

We use a partitioned target composed of ^{235}U and ^{238}U for fission cross-section measurement experiments, as shown in Figure 3, with the aim of achieving simultaneous measurement of ^{235}U and ^{238}U. The substrate of the target is 80 μm thick aluminum with a diameter of approximately 32 mm. We use a full electroplating process to deposit multiple elements onto the same substrate. The entire target is divided into four regions, each with a quarter circle shape and a radius of approximately 15 mm. There is a distance of approximately 1 mm between the target area and the edge of the substrate. ^{235}U and ^{238}U are deposited on the diagonal areas of the substrate, respectively. The thickness unevenness and purity of the target are 8% and 99.9%. Polyethylene will be deposited in the area corresponding to ^{235}U and ^{238}U on the back of the substrate, which will be prepared for measuring recoil protons later.

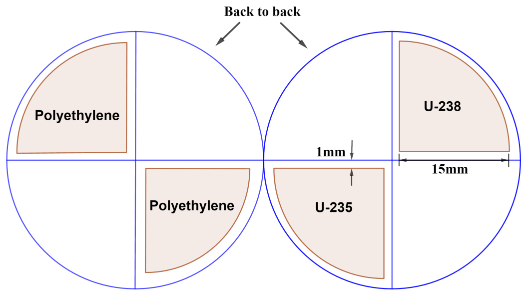

Fig. 3. The structure of the partitioned target.

In order to cover the complete particle tracks, INPC-TPC has 4608 readout pads in a single chamber, totaling over 9000 channels. This is a huge challenge for the performance of electronic systems. We conducted performance testing on the ASIC preamplifier of the TPC detector in the early stage, and its noise level was about 0.15fC/1pC (noise voltage 0.3 mV), with a dynamic range of approximately 6000:1. After connecting the data acquisition circuit, the noise of the system is about 0.6 mV, and the dynamic range is about 3000:1. The power consumption is about 10mW/Ch. The sampling frequency of the system is 50 MCPS, with 14 sampling bits. We use a RVD circuit to ensure that the voltage inside each GEM, the voltage between GEMs, and the voltage between GEMs and the readout PCB are consistent [29]. INPC-TPC collects electrons through the pad and convolves the distribution of electrons in the pad in the preamplifier to obtain the output waveform. This is different from collecting induction signals in traditional fission chambers.

The electronics system can be divided into two parts from a hardware perspective: the front-end data acquisition system and the back-end control and reception system [32]. The front-end data acquisition makes use of a standard 6U chassis, and the data transmission card serves for the input of synchronous trigger signals and the output of data. Each data acquisition card contains a total of 128 pairs of differential signal inputs. The data acquisition card communicates with the transmission card by means of a high-speed backplane to realize data exchange and command control. Furthermore, the data transmission card also undertakes the work of receiving and distributing external trigger, clock, and synchronization signals [32].

On the control side, we develop a data acquisition system

control software based on Labview. The software's functions include controlling the system's on/off, configuring parameters, monitoring the operating status of the chassis, selecting working modes, and more. We have built a real-time data monitoring and display platform based on Labview. Through this platform, we can also decode and segment the collected binary files into actual physical information, such as channel number, arrival time, signal amplitude, pulse width, and so on. The data acquisition system of INPC-TPC stores the data of each chassis separately in the form of a binary file. The sampling frequency is one point per 20 ns. The content of the file is the waveform data after packaging and assembly, and each data packet contains 128 pieces of 16-bit data. When using the packaged data, the ROOT software is used for decoding. Then we use the TTree function in ROOT for data classification, storage and retrieval.

IV. TARGET AND ELECTRONICS SYSTEMS

The main purpose of this neutron beam experiment is to test the fission fragment identification ability of INPC-TPC, so only Chamber 1 is installed, as shown in Figure 4. The partition target is fixed on the PCB center hole at the connection between the two chambers using insulation tape. The layout of the experimental site is shown in Figure 4. The neutron beam passes through different aperture neutron switch, collimator 1 and 2 to obtain beam spots of different sizes, which are then bombarded onto the target and ultimately captured by the neutron trap. We place a 6 cm thick lead brick between the neutron switch and collimator 1 to reduce the beam intensity.

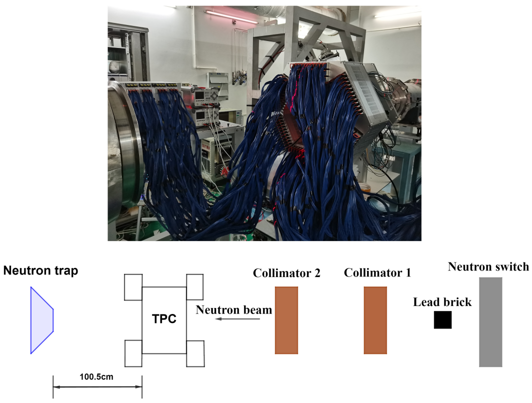

Fig. 4. The layout of the experimental site.

The working gas used in the experiment is 90% Ar+10% CF_4. The gas pressure is 100 kPa and the flow rate is 50 SCCM. The cathode voltage is -2950 V, the GEM voltage is -1280 V, and the anode PCB voltage is 0 V. The data collection threshold is 30 mV. The size of the neutron beam spot selected in the experiment is Φ30 corresponds to a neutron flux of approximately $6.1 \times 10^5 (cm^2/s)$. The proton pulse operation mode is a dual beam cluster mode. This experiment is conducted in a double-bunch mode. In the normal operation mode of CSNS, there are two proton bunches having a time interval of 410 ns in each pulse, and the repetition frequency of the pulse is 25 Hz [33].

V. PROCESSING METHODS FOR MULTI-TRACK EVENTS

Due to the wide energy range of white light neutrons, some high-energy neutrons bombard the target, substrate, or GEMs, producing various types of particles. Therefore, in white light neutron mode, there may be more than one particle track in a single event. For the case where multiple particle tracks are superimposed in the same event, we need to separate each track in the event and analyze them one by one.

Firstly, we reconstruct all tracks in all events. In this study, the reconstruction algorithm used is the 3D Iterative Hough Transform put forward by Christoph Dalitz et al. [34]. This algorithm uses spherical tessellation to discretize the parameter space. Compared with the direct discretization of the parameter space, this method can achieve better line reconstruction results. The main steps for using this algorithm to perform line detection in point clouds are as follows.

1) Input point clouds $X = \{\vec{x_1}, ..., \vec{x_n}\}$;
2) Discretize all lines passing through the three-dimensional space of the point cloud in the parameter space;
3) Perform Hough transform on point cloud X;
4) Find the line parameter corresponding to the accumulator unit with the highest number of votes;
5) Count all the points whose distances to the line are less than the width of the cell (or the threshold);
6) Fit the optimal line using the orthogonal least square method;
7) Remove the points that have been used for least squares fitting from the accumulator;
8) Repeat steps 3 to 7 until either there are too few points within X or the predetermined number of lines has been found.

For the discretization of the parameter space, this algorithm adopts the Tessellation of Platonic Solids proposed by Jeltsch et al. [35]. The number of vertices of a Platonic solid is limited. The solid with the most vertices is the icosahedron, which has 12 vertices. If we inlay a point at the center between vertices, we can obtain more vertices, and the discretized space will be more detailed. After multiple inlays, the polyhedron approaches a sphere more and more, and at this time, the degree of discretization fineness is also the highest. However, it also requires higher computational memory and significantly reduces computing speed. Therefore, it is

necessary to select an appropriate number of inlays to discretize the parameter space. In this experimental calculation, the number of inlays we adopt is 4.

One drawback of this reconstruction algorithm is that it treats all input points as equivalent. But in reality, the amplitude of each point is different, and particle tracks tend to be more biased towards points with larger amplitudes. We need to incorporate weight correction into the reconstruction algorithm. We use the signal amplitude of each point as a weight and use Weighted Least Squares (WLS) to modify the Hough transform results [29].

After reconstruction, we can obtain the line equation for each track. For a certain line L in the event,

$$L : \begin{bmatrix} x \\ y \\ z \end{bmatrix} = \begin{bmatrix} a_x \\ a_y \\ a_z \end{bmatrix} + t \begin{bmatrix} b_x \\ b_y \\ b_z \end{bmatrix} \tag{2}$$

we use the following formula to calculate the distance between each point in the event and the line L,

$$d = \sqrt{\Delta x^2 + \Delta y^2 + \Delta z^2 - (\Delta x \cdot b_x + \Delta y \cdot b_y + \Delta z \cdot b_z)^2} \tag{3}$$

$$\Delta x = a_x - x_0, \Delta y = a_y - y_0, \Delta z = a_z - z_0 \tag{4}$$

where d is the distance from a point to the line L, and (x_0, y_0, z_0) is the coordinate of the point. For points close to the line, their distance from the line is definitely smaller compared to other points. Taking the first image in Figure 5 as an example, we calculate the distance from each point to each line. Then we set a threshold and consider points with a distance less than the threshold as points on the line. We use the diameter of two and a half pads as the distance threshold (5 mm). The reconstruction and splitting results of tracks in an event are shown in Figure 5. The coordinates of the Z-axis in the figure are relative positions.

After obtaining the linear equation for each track, we need to calculate the starting and ending positions of the track in order to calculate its length. In TPC, the electron that ionizes from a particle and reaches the readout plate at the latest (with the max arrival time) is the electron that was ionized from the particle at the beginning, and its corresponding coordinate is the starting point of the track. The opposite is the ending point of the track. We find the coordinates of the point with the max arrival time in the track, and then draw a perpendicular line to the reconstructed line. The intersection point of the perpendicular line and the reconstructed line is approximately considered as the starting point of the track, which is the initial ionization position. The termination position of ionization can also be obtained using the same method. With the coordinates of the starting and ending points of the track, the length of the track can be calculated.

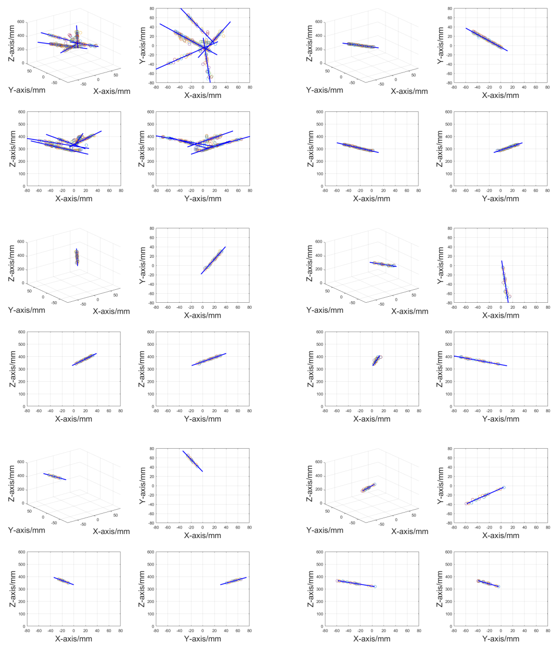

Fig. 5. The result of track processing.The first image shows the original reconstruction result, and the following ones are the results after splitting.

VI. DETECTION OF FISSION FRAGMENTS

After using the method in the previous section for track reconstruction and splitting, we obtained all particle tracks in Chamber 1. We calculate the starting point, ending point, and length of each track based on the line equation of the track. "Starting point" represents the point closest to the target in the track, while "ending point" represents the point closest to the upper GEM. We sum up the integral amplitude of all points in each track to obtain the energy (represented by the number of channels) of that track, and thereby draw a 2D statistical graph of energy and length, as shown in Figure 6(a). This result is very similar to the one measured by NIFFTE TPC [16]. We can clearly identify fission fragments from the graph. In Figure 6(a), p represents the proton, which may originate from the reaction between neutrons and detector materials or GEMs. The track length of p^* is concentrated around 70 mm, which is close to the length of our chamber. We speculate that some high-energy protons have longer tracks, even exceeding the length of the chamber, thus being truncated. The X part may be some lightweight charged particles, and we will conduct further experiments and analyze the specific components in detail later.

We take out the part marked as frag in Figure 6(a) and plot the starting points of their tracks into a 2D distribution statistical map, as shown in Figure 6(b). The distribution of points in the figure precisely corresponds to the shape and position of the partitioned target, further confirming that this part is fission fragments emitted from the target.

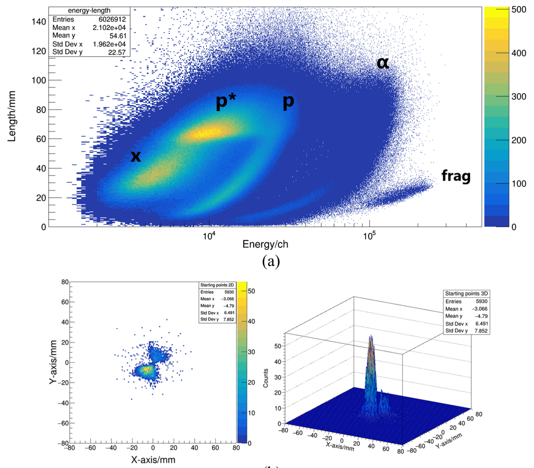

Fig. 6. Measurement results: (a) The 2D statistical graph of energy and length; (b) The 2D distribution statistical map of the starting points (frag area).

VII. MEASUREMENT OF NEUTRON BEAM SPOT

The large number of protons appearing in Chamber 1 are generated by collisions between neutrons hitting GEM or readout PCB and organic materials within them. These protons emit from the side near the GEM, and the 2D statistical distribution of their true track starting point, which is the "ending point" mentioned earlier, will be the shape of the neutron beam spot. By analyzing the 2D statistical distribution of the ending points of these tracks, the shape, size, and center position of the incident neutron beam spot can be calculated, as shown in Figure 7(a).

We project the 2D distribution statistical map onto the X-axis and Y-axis, and perform Gaussian fitting on the statistical curve, as shown in Figure 7(b). By calculating the FWHM of the fitted curve, the diameter of the neutron beam spot can be obtained as 30.52 mm (X-axis projection curve) and 29.43 mm (Y-axis projection curve). Compared to the standard diameter of 30 mm, the relative errors are 1.73% and 1.89%. The measurement accuracy is superior to the results measured by other research teams previously [36]. According to the fitting curve, the center position is calculated to be approximately (-2.52 mm, 2.04 mm). Perhaps the placement of the detector was not accurately calibrated, resulting in a deviation in the center position.

VIII. CONCLUSION AND OUTLOOK

This paper introduces a new type of TPC detector, INPC-TPC, used for fission cross-section measurement. Its core goal is to improve the accuracy of fission cross-section measurement for major actinide elements to 1% or higher. The characteristic of this TPC is the use of a larger readout detector and the clever design of a symmetrical dual-chamber structure, which enables simultaneous measurement of protons and fragments. This study is an important test of the performance of INPC-TPC. Under the wide energy range of white light neutrons, we can still efficiently identify fission fragments, demonstrating the powerful particle identification ability of INPC-TPC. In addition, we used this detector to measure the neutron beam spot, and the experimental results were very close to the reference value. Next, we will assemble Chamber 2 and conduct a neutron energy calibration experiment in single beam cluster mode. Another team of ours will measure the number of target nuclei of the reference target. We expect that an accurate measurement of the cross-section ratio of ^{235}U(n,f)/H(n,n) and ^{238}U(n,f)/H(n,n) can be finally achieved.

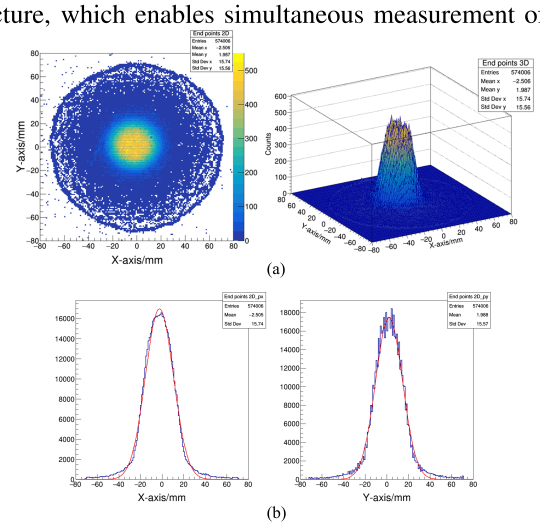

Fig. 7. Measurement results of neutron beam spot: (a) The 2D and 3D distribution statistical map of the incident neutron beam spot; (b) The projection curve of the 2D distribution map towards the X-axis and Y-axis, where the red line represents the Gaussian fitting result.

IX. ACKNOWLEDGE

The author sincerely appreciates the experimental equipment and hardware support provided by the Institute of Nuclear Physics and Chemistry, Chinese Academy of Engineering Physics. The author also thanks the Chinese Spallation Neutron Source for providing experimental conditions and technical support. This work was performed under the auspices of the Youth Doctoral Talent Incubation Program of the Second Affiliated Hospital of Army Medical University (grant no. 2024YQB060).

[1] M. Heffher, D.M. Asner, R.G. Baker, *et al.*, A Time Projection Chamber for High Accuracy and Precision Fission Cross Section Measurements. Nucl. Instrum. Methods Phys. Res., Sect.

A. **759**, 50–64 (2014). doi: 10.1016/j.nima.2014.05.057

[2] G. Aliberti, G. Palmiotti, M. Salvatores, *et al*., Nuclear data sensitivity, uncertainty and target accuracy assessment for future nuclear systems. Ann. Nucl. Energy. **33**, 700–733 (2006). DOI: 10.1016/j.anucene.2006.02.003

[3] D.R. Nygren, Origin and development of the TPC idea. Nucl. Instrum. Methods Phys. Res., Sect. A. **907**, 22–30 (2018). DOI: 10.1016/j.nima.2018.07.015

[4] T. Medcalf, M.R. Saich, J.A. Strong, A dedicated TPC track processor for the Aleph second level trigger. Nucl. Instrum. Methods Phys. Res., Sect. A. **277**, 358–367 (1989). DOI: 10.1016/0168-9002(89)90764-X

[5] P. Delpierre, The DELPHI TPC. Nucl. Instrum. Methods Phys. Res. **225**, 566–574 (1984). DOI: 10.1016/0167-5087(84)90106-6

[6] H. Wieman, E. Anderssen, STAR TPC at RHIC. IEEE Trans. Nucl. Sci. **44**, 671–678 (1997). DOI: 10.1109/23.603731

[7] P. Glässel, The ALICE TPC—An innovative device for heavy ion collisions at LHC. Nucl. Instrum. Methods Phys. Res., Sect. A. **572**, 64–66 (2004). DOI: 10.1016/j.nima.2006.10.347

[8] R. Diener, J. Dreyling-Eschweiler, H. Ehrlichmann et al., The DESY II test beam facility. Nucl. Instrum. Methods Phys. Res., Sect. A. **922**, 265–286 (2019). DOI: 10.1016/j.nima.2018.11.133

[9] D. Attié, T. Behnke, A. Bellerive et al., A time projection chamber with GEM-based readout. Nucl. Instrum. Methods Phys. Res., Sect. A. **856**, 109–118 (2017). DOI: 10.1016/j.nima.2016.11.002

[10] S.B. Wang, D. Bernard, H. Ohkuma et al., HARPO: beam characterization of a TPC for gamma-ray polarimetry and high angular-resolution astronomy in the MeV-GeV range. Journal of Physics: Conference Series. **650**, 012016 (2015). DOI: 10.1088/1742-6596/650/1/012016

[11] J.Y. Yuan, Y. Qian, H.Y. Zhao et al., Development of multichannel readout electronics prototype system for TPC detector of CSR External-Target Experiment. Nucl. Instrum. Methods Phys. Res., Sect. A. **1052**, 168281 (2023). DOI: 10.1016/j.nima.2023.168281

[12] H. Li, S. Zhang, F. Lu et al., Momentum resolution simulation of time projection chamber of Lanzhou heavy ion storage ring outer target experimental terminal. Nuclear Techniques. **39**, 070401 (2016). DOI: 10.11889/j.0253-3219.2016.hjs.39.070401

[13] S.B. Wang, PandaX-III high pressure xenon TPC for Neutrinoless Double Beta Decay search. Nucl. Instrum. Methods Phys. Res., Sect. A. **958**, 162439 (2020). DOI: 10.1016/j.nima.2019.162439

[14] X. Chen, C.B. Fu, J. Galan et al., PandaX-III: Searching for neutrinoless double beta decay with high pressure ^{136}Xe gas time projection chambers. Sci. China Phys. Mech. Astron. **60**, 061011 (2017). DOI: 10.1007/s11433-017-9028-0

[15] J. Pan, Z.Y. Zhang, C.Q. Feng et al., An ultra-low background alpha detection system with a Micromegas-based time projection chamber. Rev. Sci. Instrum. **93**, 013303 (2022). DOI: 10.1063/5.0070612

[16] R.J. Casperson, D.M. Asner, J. Baker et al., Measurement of the ^{239}Pu(n,f)/^{235}Ue(n,f) Cross-Section Ratio with the NIFFTE fission Time Projection Chamber. Phys. Rev. C. **97**, 034618 (2018). DOI: 10.1103/PhysRevC.97.034618

[17] M. Monterial, K.T. Schmitt, C. Prokop et al., Measurement of material isotopics and atom number ratio with α-particle spectroscopy for a NIFFTE fission Time Projection Chamber actinide target. Nucl. Instrum. Methods Phys. Res., Sect. A. **1021**, 165864 (2022). DOI: 10.1016/j.nima.2021.165864

[18] L. Snyder, D.M. Asner, R.G. Baker et al., Measuring the α/SF Branching Ratio of ^{252}Cf with the NIFFTE TPC. Nucl. Data Sheets. **119**, 386–388 (2014). DOI: 10.1016/j.nds.2014.08.107

[19] Y. Li, H. Yi, Y.K. Sun et al., Performance study of the Multi-purpose Time Projection Chamber (MTPC) using a four-component alpha source, Nucl. Instrum. Methods Phys. Res., Sect. A. **1060**, 169045 (2024). DOI: 10.1016/j.nima.2023.169045

[20] Z. Chen, C. Feng, H. Chen et al., Readout system for a prototype multi-purpose time projection chamber at CSNS Back-n, J. Instrum. **17**, P05032 (2022). DOI: 10.1088/1748-0221/17/05/p05032

[21] R.R. Fan, Q. Li, J. Bao et al., Detector development at the Back-n white neutron source. Radiation Detection Technology and Methods. **7**, 171–191 (2023). DOI: 10.1007/s41605-022-00379-5

[22] H.F. Bai, H. Yi, Y.K. Sun et al., Measurement of cross section for the ^{232}Th(n, f) reaction using a time projection chamber, Nucl. Instrum. Methods Phys. Res., Sect. A. **1058**, 168912 (2024). DOI: 10.1016/j.nima.2023.168912

[23] H.F. Bai, H. Yi, Y.K. Sun et al., Cross section measurement for the ^{232}Th(n, f) reaction in the 4.50-5.40 MeV region using a time projection chamber. Chinese Phys. C. **48**, 104001 (2024). DOI: 10.1088/1674-1137/ad5ae6

[24] P. Marini, L. Mathieu, M. Aïche et al., Development of a Gaseous Proton-Recoil Detector for neutron flux measurements between 0.2 and 2 MeV neutron energy. EPJ Web Conf. **211**, 03010 (2019). DOI: 10.1051/epjconf/201921103010

[25] J. Wei, S.N. Fu, J.Y. Tang et al., China Spallation Neutron Source - an overview of application prospects. Chinese Phys. C. **33**, 1033–1042 (2009). DOI: 10.1088/1674-1137/33/11/021

[26] 26. H.Y. Dong, H. Song, Q. Li et al., The vacuum system of the China spallation neutron source. Vacuum. **154**, 75–81 (2018). DOI: 10.1016/j.vacuum.2018.04.046

[27] H.S. Chen, Y.B. Chen, F.W. Wang et al., Target station status of China Spallation Neutron Source. Neutron News. **29**, 2–6 (2018). DOI: 10.1080/10448632.2018.1514186

[28] J.Y. Tang, Q. An, J.B. Bai et al., Back-n white neutron source at CSNS and its applications. Nucl. Sci. Tech. **32**, 11 (2021). DOI: 10.1007/s41365-021-00846-6

[29] J.J. Zhang, J. Xiao, J.J. Sun et al., Identification of α particles and fission fragments emitted by ^{252}Cf using a fission time projection chamber. Radiat. Meas. **174**, 107126 (2024). DOI: 10.1016/j.radmeas.2024.107126

[30] Y.F. Lai, Y.L. Li, Y.J. Li et al., Experimental Study on the Performance of Tri-GEM Gas Detector. High Energy Physics and Nuclear Physics. **30**, 767–770 (2006). DOI: 10.1016/S1872-2040(06)60029-7

[31] Y.Y. Yan, Y.L. Li, M. Huang et al., The design of time projection chamber for fission cross-section measurements. NSS/MIC/RTSD. 1–3 (2016). DOI: 10.1109/NSS-MIC.2016.8069851

[32] J.J. Zhang, J. Xiao, J.J. Sun et al., Determination of the number of ^{235}U target nuclei in the irregular target using a fission time projection chamber. Nucl. Eng. Technol. **56**, 444–450 (2024). DOI: 10.1016/j.net.2023.10.017

[33] H. Yi, T.F. Wang, Y. Li et al., Double-bunch unfolding methods for the Back-n white neutron source at CSNS. J. Instrum. **15**, P030326 (2020). DOI: 10.1088/1748-0221/15/03/P03026

[34] C. Dalitz, T. Schramke, M. Jeltsch, Iterative Hough Transform for Line Detection in 3D Point Clouds. Image Processing On Line. **7**, 184–196 (2017). DOI: 10.5201/ipol.2017.208

[35] M. Jeltsch, C. Dalitz, R. Pohle-Fröhlich, Hough Parameter Space Regularisation for Line Detection in 3D. Conference: International Conference on Computer Vision Theory and Applications. 345–352 (2016). DOI: 10.5220/0005679003450352

[36] C.C. Han, X.P. Ouyang, X.P. Zhang, Measurement of Beam Profile of CSNS Back-n. Atomic Energy Science and Technology. **54**, 386–393 (2020). DOI: 10.7538/yzk.2019.youxian.0481